Hueckel, T. *et al.* (2011). *Géotechnique* **61**, No. 10, 831–844 [http://dx.doi.org/10.1680/geot.9.P.124]

Temperature-dependent internal friction of clay in a cylindrical heat source problem

T. HUECKEL*, B. FRANCOIS† and L. LALOUI‡

The effect of the temperature dependence of the internal friction angle is studied in a boundary value problem simulating the impact of a cylindrical heat source on the soil mass in which it is embedded. This follows a previous study which shows that such temperature dependence may substantially affect the interpretation of thermal failure in laboratory experiments. Even if the thermal increase of the internal friction is quite modest (less than 20% in terms of the critical state parameter, M), it affects quite significantly the effective stress path near the heat source. The effective stress path approaches the yield locus and the critical state at significantly higher principal stress difference values for the variable internal friction than for the $M = \text{const}$ case. The 'mean effective stress distance from the critical state' is substantially reduced during heating, which in the case of small perturbations of any parameter may lead to potentially unstable or statically inadmissible behaviour. The solutions obtained allow one to identify zones of influence around the heat source of several variables of interest. The two fields most affected by the thermal sensitivity of M are that of the axial stress, dropping significantly near the heat source, and that of the appearance of the thermoplastic strain. Both zones of influence are reduced in size by almost half when the friction angle is increased by 20% over 70°. The presented results may be of relevance to the design of prototype in situ installations and their monitoring, and eventually of actual facilities for nuclear waste disposal.

KEYWORDS: clays; failure; friction; numerical modelling; temperature effects

On étudie l'effet de la température sur l'angle de frottement interne dans le cadre d'un problème aux limites simulant l'impact d'une source de chaleur cylindrique sur la masse de sol dans laquelle elle est enfuie. Cette étude fait suite à une étude précédente qui illustre la façon dont cet effet de la température risque d'affecter considérablement l'interprétation de ruptures thermiques dans le cadre d'expériences en laboratoire. Même lorsque l'augmentation thermique est plutôt modeste (moins de 20% pour le paramètre d'état critique M), elle affecte de façon significative le chemin de contraintes à proximité de la source de chaleur. Le chemin des contraintes effectives s'approche du point de plastification et de l'état critique en présence de différences de contrainte principales beaucoup plus élevées dans le cas du frottement interne variable que dans celui de M constant. La « distance entre la contrainte effective moyenne et l'état critique » se réduit de façon significative au cours du chauffage, ce qui, dans le cas de perturbations limitées d'un quelconque des paramètres, risque d'engendrer un comportement potentiellement instable ou statiquement inadmissible. Les solutions obtenues permettent d'identifier des zones d'influence autour de la source de chaleur de plusieurs variables intéressantes. Les deux champs les plus affectés par la sensibilité thermique de M sont la contrainte axiale, qui diminue sensiblement à proximité de la source de chaleur, et l'aspect de la contrainte thermoplastique. La taille des deux zones d'influence diminue presque de moitié lorsque l'angle de frottement augmente de 20% à plus de 70°C. Les résultats présentés pourront être pertinent dans l'étude et le contrôle de prototype d'installations in-situ – et éventuellement – de dispositifs de stockage de déchets nucléaires.

INTRODUCTION

The influence of temperature on internal friction angle may not be numerically large, but as demonstrated in a recent paper (Hueckel *et al.*, 2009a), a 10% temperature-induced increase in critical state coefficient $M(\Delta T)$ over 90°C leads to a complete pattern change in the triaxial compressive strength, producing an increase in its value of up to 25%, compared with the case of a temperature-independent friction angle. Experimental studies of the triaxial strength of clays show that remoulded kaolin clay and natural Boom Clay exhibit temperature dependence of their internal friction, whereas this is not the case for largely smectitic or illitic clays (Hueckel & Baldi, 1990; Hueckel & Pellegrini, 1991; Cekerevac & Laloui, 2004). Interestingly, the effects of the thermal variation of internal friction depend heavily on the history of heating and loading. In particular, the state of stress at which heating is performed, including the soil overconsolidation ratio, impacts on the ensuing variation of strength (Hueckel *et al.*, 2009a). Constitutive postulates for the thermal variation of the internal friction angle, their mathematical representation within the thermal Cam-Clay model (Hueckel & Borsetto, 1990) and their limitations are addressed by Hueckel *et al.* (2009b).

Emerging technologies concerning thermally affected soil masses often involve prototype installations, the long-term performance of which requires intense monitoring. Such technologies include: nuclear waste disposal; energy storage in subsoil using geostructures such as piles, walls and slabs; alternating seasonal heating and cooling of buildings; oil recovery from high-pressure, high-temperature reservoirs; and underground pipes and cables. The monitoring systems need to be placed in the ground early during the construction phase for such installations. Their design includes the type, sensitivity and configuration of sensors. This is based largely on numerical prediction of the evolution of variables

Manuscript received 9 October 2009; revised manuscript accepted 15 October 2010. Published online ahead of print 15 February 2011. Discussion on this paper closes on 1 March 2012, for further details see p. ii.

* Department of Civil and Environmental Engineering, Duke University, Durham, NC, USA.
† Building, Architecture and Town Planning Department (BATir), Université Libre de Bruxelles, Belgium.
‡ Laboratory of Soil Mechanics, Ecole Polytechnique Fédérale de Lausanne, Switzerland.

of interest characterising the response of the thermally affected soil mass.

This paper presents numerical investigations of the effect of temperature on the thermomechanical response of a saturated soil mass at the scale of a boundary value problem of a cylindrical heat source embedded in soil. Additional factors affect the response of the soil mass compared with the laboratory experiments. These are time-dependent heat conduction, and the permeability-dependent rate of dissipation of thermally generated pore pressure. The presented solution shows the utility of numerical predictions aimed at optimisation of the monitoring systems and devices. It demonstrates the predictive capabilities of the numerical simulator, and points to various consequences of temperature-dependent friction angle affecting the field of stress and displacement components, pore water pressure and water flow rate components in functionally selected locations and possible points of special interest. Notably, it shows that the role of the friction angle is not limited to the failure states, but that, as it controls the shape of the yield locus prior to reaching failure state, it is also important for the entire pre-failure elasto-plastic process.

OUTLINE OF THE MODEL

The central assumption of the model is that the critical state parameter M representing the internal friction angle, ϕ', is a function of temperature difference with respect to the reference temperature T_0, $\Delta T = T - T_0$ (Laloui, 1993). All quantities marked with a subscript '0' are the values at the reference state.

$$\begin{aligned} M &= M_0 + g\Delta T \\ M &= \frac{6\sin\phi'}{3-\sin\phi'} \\ M_0 &= \frac{6\sin\phi'_0}{3-\sin\phi'_0} \end{aligned} \tag{1}$$

where the coefficient g is constant. The variation of M affects the evolution of the yield locus, chosen here as the classical Cam-Clay form (Schofield & Wroth, 1968), changing mainly its aspect ratio, $q_{\max}/p'_{\max}$,

$$f = \frac{q}{Mp'} + \ln\left(\frac{2{\cdot}718\,p'}{p'_c}\right) - 1 = 0 \tag{2}$$

where p' and q are the mean and deviatoric effective stress invariants. Stresses are considered positive when compressive.

The other parameter controlling the locus evolution is the apparent preconsolidation pressure p'_c, which depends on the accumulated irreversible volumetric plastic strain and temperature, represented here by a specific function originated by Laloui & Cekerevac (2003),

$$p'_c = p'_{c0}\exp\left(\beta\varepsilon_v^p\right)\left[1-\gamma\log\left(1+\frac{\Delta T}{T_0}\right)\right] > 0 \tag{3}$$

where p'_{c0} is an initial preconsolidation pressure, usually referred to the in situ state, and γ and β are constitutive coefficients of thermal softening and of isothermal isotropic irreversible compression.

The hypo-elastic (incrementally reversible) part of the strain increment is expressed as

$$\begin{aligned} \mathrm{d}\varepsilon_v^e &= \frac{1}{K}\mathrm{d}p' - \beta'_s\mathrm{d}T \\ \mathrm{d}\varepsilon_d^e &= \frac{1}{3G}\mathrm{d}q \end{aligned} \tag{4}$$

where the volumetric and deviatoric elastic strain invariants are defined as

$$\begin{aligned} \varepsilon_v^e &= \varepsilon_1^e + \varepsilon_2^e + \varepsilon_3^e; \\ \varepsilon_d^e &= \left(\tfrac{2}{3}e_{ij}^e e_{ij}^e\right)^{1/2}; \\ e_{ij}^e &= \varepsilon_{ij}^e - \tfrac{1}{3}\varepsilon_{kk}^e\delta_{ij} \end{aligned} \tag{5}$$

where K and G are the incremental bulk and shear hypo-elasticity moduli respectively. To reflect their well-known and pronounced variability with the depth in situ, they are both postulated as functions of p'

$$\begin{aligned} K &= K_{\mathrm{ref}}\left(p'/p'_{\mathrm{ref}}\right)^{n'} \\ G &= G_{\mathrm{ref}}\left(p'/p'_{\mathrm{ref}}\right)^{m'} \end{aligned}$$

where p'_{ref} is the reference pressure at which K_{ref} and G_{ref} are measured (Hujeux, 1985; Laloui & François, 2009). β'_s is the volumetric thermal (reversible) expansion coefficient of the solid skeleton.

From the analyses presented in Hueckel *et al.* (2009a), it transpires that in a process of continuous (thermoplastic) yielding during heating, an interesting balance of plastic straining, temperature change and effective stress change arises, driven by the balance between the various components of hardening contributions, and expressed through Prager's consistency equation for thermoplasticity (Prager, 1958; Hueckel & Borsetto, 1990)

$$\begin{aligned} \mathrm{d}f = \frac{\partial f}{\partial \underset{\sim}{\sigma}'}:\mathrm{d}\underset{\sim}{\sigma}' \\ + \frac{\partial f}{\partial p'_c}\left(\frac{\partial p'_c}{\partial \varepsilon_v^p}\mathrm{d}\varepsilon_v^p + \frac{\partial p'_c}{\partial T}\mathrm{d}T\right) + \frac{\partial f}{\partial M}\frac{\partial M}{\partial T}\mathrm{d}T = 0 \end{aligned} \tag{6}$$

When temperature is controlled, as in a homogeneously heated specimen, under constant stress, a one-to-one relationship can be established between temperature history and the resulting thermoplastic strain. Various examples of such processes and corresponding experimental data have been discussed for homogeneous, homogeneously stressed and homogeneously heated specimens by Hueckel *et al.* (2009a), showing characteristic patterns of behaviour for both drained and undrained conditions.

In the present study, which focuses on analogous phenomena, but on a larger scale of a boundary value problem, the process is additionally affected by non-uniform and time-dependent effects of heat conduction, resulting in a non-uniform distribution of temperature, thermal expansion of water, and ensuing pore water pressure change, triggering in turn a flux of pore water and time-dependent dissipation of pore pressure. The pore pressure is clearly coupled, by way of the effective stress principle, with the evolution of the effective stress. In addition, the evolution of pore water pressure is constrained by the thermally induced volumetric strains of the porous soil skeleton, under both thermoelastic (expansive) and thermoplastic (contractile) regimes.

THERMOPLASTIC BOUNDARY VALUE PROBLEM

The thermo-hydro-mechanical response of a soil mass around a cylindrical heat source has been the subject of

numerous studies in the past, with different levels of complexity, from the classical analytical thermoelastic solution of Goodier (1937) (see also Timoshenko & Goodier, 1934), through other analytical solutions for various thermal loadings (Booker & Savvidou, 1985; McTigue, 1986; Zhou *et al.*, 1998) to more recent finite element computations including thermoelasticity (Britto *et al.*, 1989; Carter & Booker, 1989) or thermoplasticity (Hueckel *et al.*, 1987; Borsetto *et al.*, 1993; Giraud, 1993; Ma & Hueckel, 1993; Picard, 1994; Seneviratne *et al.*, 1994; François *et al.*, 2009). In the present study an isolated vertical cylindrical heat source is considered, and its thermo-hydro-mechanical effects on the surrounding clay mass are studied. The soil material of choice is Boom clay, a possible host formation for nuclear waste disposal in Belgium, and well characterised from both the mechanical and thermomechanical points of view (Baldi *et al.*, 1991; Hueckel & Pellegrini, 1992; see also Hueckel *et al.*, 2009a).

The finite-element method was chosen to study the global coupled thermo-hydro-mechanical processes governing the phenomena. The field equations considered represent the medium as a deformable two-phase material (i.e. a water-saturated medium), in which heat and mass transfers occur (Lewis & Schrefler, 1987; Olivella *et al.*, 1994; Gawin *et al.*, 1995; Collin *et al.*, 2002). ACMEG-T, which is an elasto-thermoplastic constitutive model (Laloui & François, 2009) that can be simplified to a thermal Cam-Clay model (equations (1)–(4)) as a particular case, has been implemented in the finite-element code LAGAMINE, developed at Liège University (Charlier, 1987; Charlier *et al.*, 2001; Collin, 2003). Readers interested in the finite-element formulation of the LAGAMINE code may refer to Collin *et al.* (2002).

Eight-node, two-dimensional, large-strain finite elements are used. Such elements possess five degrees of freedom at each node: two solid displacements, liquid water pressure, gas (dry air + vapour) pressure, and temperature. Nevertheless, the gas pressure is not considered as a degree of freedom, because water saturation conditions are assumed all along the THM processes.

A horizontal unit height slice of Boom clay is considered, placed in the mid-plane of the heating source. The slice is meshed, assuming radial (horizontal) propagation of thermal and hydraulic fluxes as well as the plane-strain configuration (no vertical deformation). The computation domain is axisymmetric around the vertical axis of the heat source (Fig. 1). The heater has an interface with soil at a radius of 0·095 m. The modelled domain is contained between the internal boundary, corresponding to the external radius of the heater, and an external, fictitious boundary, which is placed at a sufficient distance (100 m) to limit as much as possible its location influence on the computation results.

Although the boundary value problem chosen is very simple (axial symmetry, plane strain), it epitomises many of characteristics of the fully developed 'realistic' field problems.

The initial conditions for the boundary value problem are chosen to replicate those for the planned repository in Boom Clay, and are reported in Table 1 (François *et al.*, 2009). As expounded in Hueckel *et al.* (2009a), the thermomechanical response of clays is heavily dependent on the mechanical and thermal history of the material. Thus it is desired to represent the pre-simulation history of the soil mass as faithfully as possible.

The initial state is defined as follows. The initial in situ Boom Clay stress state is reproduced as slightly anisotropic, with $K_0 = 0{\cdot}8$ under the assumption that $\sigma_r = \sigma_t$ (see Table 1). The initial overconsolidation ratio of the clay is about 2·4: hence the initial stress state is elastic. This state of stress, and that of zero initial (pre-induced) plastic strain, does not account for possible changes in those variables (and permeability) induced by both the excavation stress relief and damage. No established data on these effects are available at present.

The heating phase consists in a gradual increase of temperature from 16·5°C (i.e. in situ temperature of Boom Clay at the level of the HADES underground laboratory) to 96·5°C within 30 days. Then a constant temperature of

Table 1. Initial state of Boom Clay considered in the computations.

Variable	Value
Vertical total stress, σ_z: MPa	4·87
Horizontal total stress, $\sigma_r = \sigma_t$: MPa	4·30
Pore water pressure, p_w: MPa	2·02
Vertical effective stress, σ'_z: MPa	2·85
Horizontal effective stress, $\sigma'_r = \sigma'_t$: MPa	2·28
Mean effective stress, p': MPa	2·47
K_0	0·8
Initial preconsolidation pressure, p'_{c0}: MPa	6
Temperature, T: °C	16·5
Initial void ratio, e_0	0·6

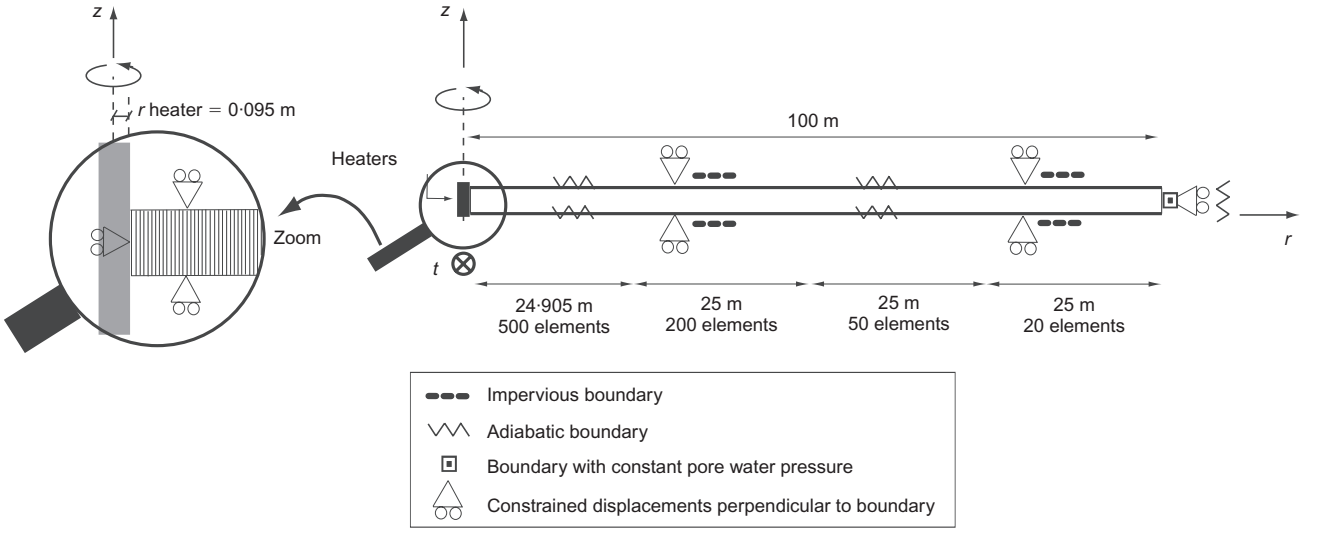

Fig. 1. Modelled domain and boundary condition in the *r* (radial), *t* (circumferential) and *z* (axial) axis system. Details of the finite-element size

96·5°C is maintained for 2 years. In terms of numerical solutions, the relatively low velocity of the thermal loading with respect to the size of the mesh and the permeability of the medium avoids any numerical oscillations of the pore pressure, without requiring specific stabilisation techniques.

The boundary conditions are summarised in Table 2 and Fig. 1.

Tables 3 and 4 report the mechanical and diffusive material parameters respectively. The permeability of water, k, is assumed to be dependent on water viscosity μ_w, $k = k_w/\mu_w$, which in turn is a function of temperature (Table 4). The thermal expansion coefficient of pore water is also assumed to be constant and equal to that of tap water. The effects of non-linearity of the thermal expansion coefficient and those of the presence of adsorbed water (Baldi *et al.*, 1988) are neglected. Boom Clay exhibits an increase of M with temperature (from 0·8 at 16·5°C to 1·16 at 96·5°C), resulting in a positive parameter g.

Table 2. Thermo-hydro-mechanical boundary conditions of the modelled domain

	Mechanical	Hydraulic	Thermal
$r = 0{\cdot}095$ m	$u_r = 0$	No flux	$T = T_{imp}$
$r = 100$ m	$u_r = 0$	$p_w = p_w$ in situ	No flux
Lateral	$u_z = 0$	No flux	No flux

Table 3. Mechanical parameters of Boom Clay used in computations

Parameter	Value
Elastic parameters	
K_{ref}: MPa	130
G_{ref}: MPa	130
n'	0·4
m'	0·4
β_s': °C^{-1}	5×10^{-5}
Isotropic plastic parameters	
β	16
γ	0·55
Deviatoric plasticity parameters	
ϕ_0': degrees	20·6
g	$4{\cdot}5 \times 10^{-3}$

Table 4. Thermal and hydraulic diffusion parameters of Boom clay used in computations

Parameter	Value
ρ_{w0}: kg/m^3	1000
ρ_s: kg/m^3	2670
n	0·39
k_w: m^2	2×10^{-19}
χ_w: Pa	$2{\cdot}2 \times 10^{9}$
β_w': °C^{-1}	$3{\cdot}5 \times 10^{-4}$
μ_{w0}: Pa.s	0·001
α_T: °C^{-1}	0·011
$c_{p,w}$: J.kg/°C	4186
$c_{p,s}$: J.kg/°C	732
λ_w: W/(m °C)	0·57
λ_s: W/(m °C)	2·42

Values extracted from SCK-CEN (1997), Bastiaens *et al.* (2006) and Bernier *et al.* (2007) (see also François *et al.*, 2009).
Subscripts w and s refer to water and solid respectively. Water viscosity, $\mu_w = \mu_{w0}[1 - \alpha_T(T - T_0)]$; μ_{w0} and α_T are material constants; thermal diffusivity, $\Gamma = n\lambda_w + (1 - n)\lambda_s$. n is the porosity.

RESULTS AND DISCUSSIONS

Pore water pressure and flux

Given the very low permeability of Boom Clay, the short-term response of the field around the heat source develops in conditions very close to undrained ones. Hence, as there is very little water outflow, the pore water pressure evolution is controlled mainly by the difference between the thermal expansion of water and the much smaller expansion of the solid skeleton. This produces a pore water pressure increase, initially following a familiar, highly localised temperature distribution around the heat source until about 50 days of heating (Figs 2(a) and 2(b)). In this initial period of about 2 months, the temperature and pore pressure affect a limited volume of soil, not exceeding 1·5 m in radius. However, in a later period, the pore pressure increase covers a much wider zone than the temperature. More than a 1·5 MPa water pressure growth is seen in the volume of diameter nearly 6 m (Fig. 2(b)). Also, in the later stage, the effects of the hydraulic boundary condition at the source/soil interface of no flux are felt more strongly than initially, resulting in a pore pressure gradient that is nearly zero (but is never negative, as it would be in the case of cooling following the heating period), and hence in virtually no flow near the source. Notably, near the source the pore pressure value starts to decrease, after reaching a maximum value at about 50 days (Figs 2(c) and 3(b)). In contrast, in a more remote range at more than about $r = 1{\cdot}75$ m, the trend is opposite: the pore pressure grows monotonically. The transition point between these two types of evolution corresponds approximately to a zero curvature point (as in the one-dimensional consolidation equation), which also is approximately the location of the maximum water flux point (Fig. 3(a)). As seen, the flux is initially in a classical form of front, whereas later it diffuses. This has very important implications for potential mass transport of a possible prematurely released radioactive contaminant in a nuclear waste repository. Because of such a low thermally activated water flux in the vicinity of the heat source, the possible radionuclide transport would then occur almost entirely through diffusion, with minimal enhancement through advection (which would in any case be subsequently inverted during cooling, which is not considered here).

The influence of mechanics on the thermal field is known to be very limited, as it is induced via changes in porosity. As these changes are small, the temperature distribution seems to be independent of deformation, and of whether M is constant or variable (Fig. 2(a)). This is not exactly the case for pore pressure (Figs 2(b) and 2(c)).

Pore pressure is generated by the differential expansion of water and clay solids, which enclose the pore containing water. The expansion of the solid skeleton is either smaller than that of water, or even negative, in the case of thermo-plastic collapse (Fig. 4). Total volumetric deformation is clearly dominated by the thermoelastic strain, again with the difference determined by the extent of the elastic range affected by the evolution of M.

A limited dependence on the internal friction variation is seen, as explained below. Notably, the episode of plastic strain change is very short in time.

The pore pressure evolution in time near the heat source (Fig. 3(b)) for the case $M = 0{\cdot}8 = \text{const}$ (that for a variable M differs only slightly) shows a process that is quite uniform spatially, with the differences in terms of the pressure value at a given moment being of the order of 0·1 MPa. Despite

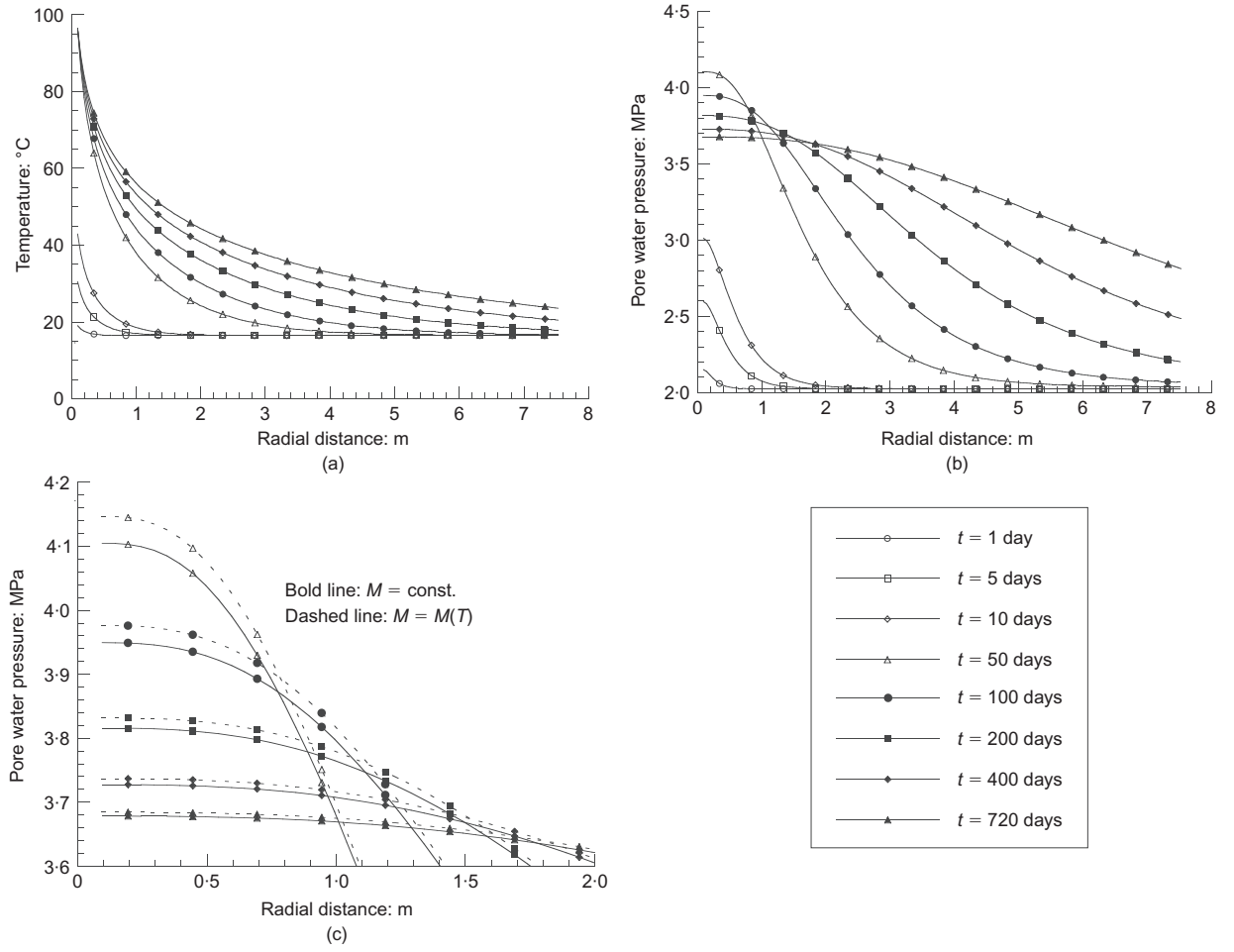

Fig. 2. Evolution of: (a) temperature (identical for both $M = \text{const}$ and $M(\Delta T)$); (b) pore water pressure distribution around heat source (negligible dependence on $M(\Delta T)$ over most of field); (c) pore water pressure in closest vicinity of heat source, showing limited dependence on M

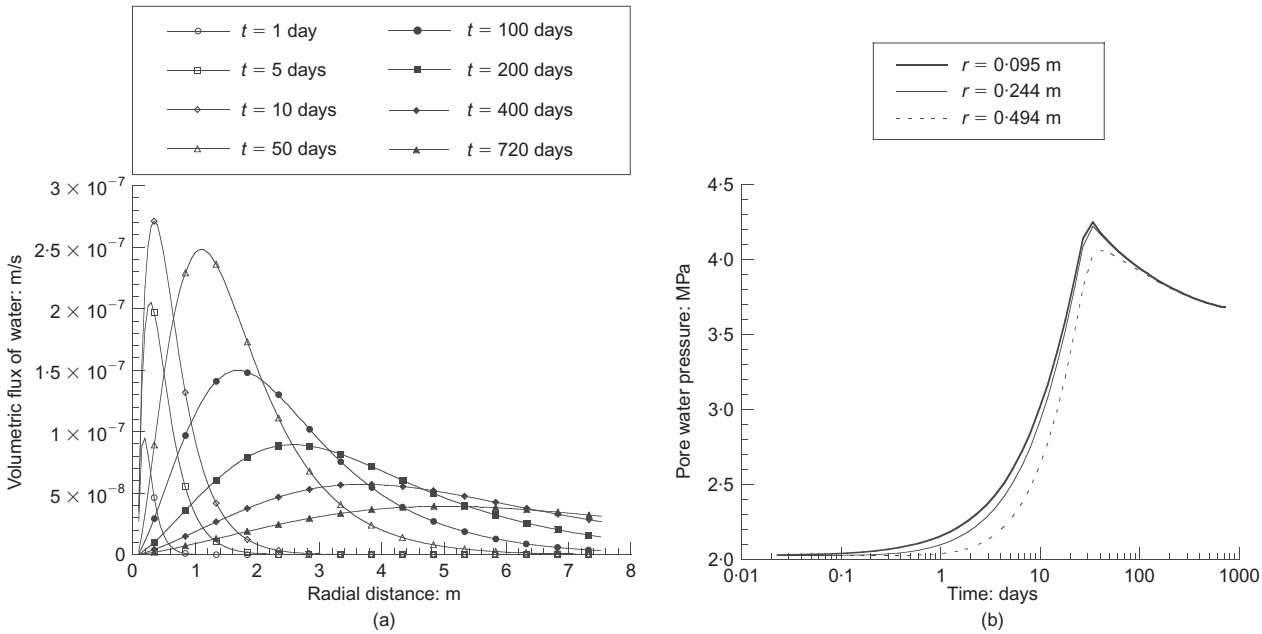

Fig. 3. For $M = 0{\cdot}8 = \text{const}$: (a) evolution of volumetric flux of water; (b) evolution of pore pressure with time at $r = 9{\cdot}5$ cm, 24·4 cm and 50·4 cm (0 cm, 14·9 cm and 40·9 cm from heat source perimeter)

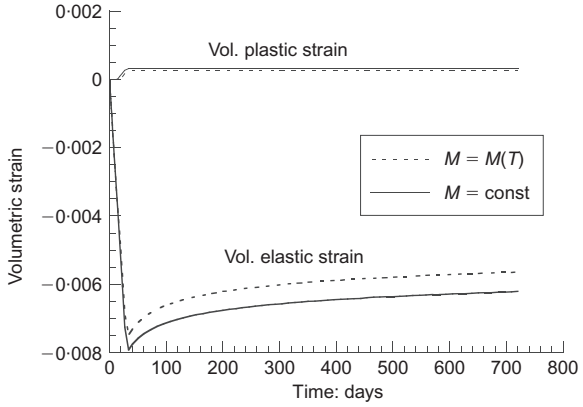

Fig. 4. Evolution of volumetric elastic and plastic strains at $r = 15{\cdot}5$ cm (= 6 cm from heat source perimeter) for constant and variable M

this relative uniformity of pore pressure, the effective stress evolution exhibits quite a different pattern.

Effective and total stress trajectories

The relatively weak dependence of pore pressure on the variations of the internal friction (or M) can be best explained by considering its coupling to the effective stress evolution. Understanding the effective stress trajectory, particularly near the heat source, is crucial from the point of view of the stress analysis and structural safety of the soil mass supporting the heat source thermally and structurally.

To start with, it should be reiterated that the principal stress directions are: parallel to the symmetry axis, along the radius and tangential to the circumferential coordinate. Second, all the material behaviour characteristics are assumed to be independent of the third effective stress invariant (or Lode angle, θ_L), but the plane-strain states are not. Therefore, a proper representation of stress trajectories is provided in what follows in q, p', θ_L space, while the yield locus and critical state locus are independent of θ_L. The Lode angle, $0 < \theta_L < 60°$ (following Chen & Han, 1988, but using the compression-positive sign convention), measures a declination on the octahedral plane, $\sigma'_1 + \sigma'_2 + \sigma'_3 = \text{const}$, from the direction of the major principal compressive stress. $\theta_L = 0°$ corresponds to the case $\sigma'_2 = \sigma'_3$, and $\theta_L = 60°$ is reached for $\sigma'_1 = \sigma'_2$.

The effective stress field arises in response to the thermal pore pressure generation, subjected to the constraints of equilibrium and boundary conditions imposed on the total stress field. Therefore, the effective stress field evolution in the first (immediate, nearly undrained) stage is, like that of the pore pressure field, controlled mainly by the heat diffusion or temperature field evolution. In a later, much slower and longer phase, owing to a decreasing pore pressure gradient (see Fig. 3(a)), the controlling factor becomes the (very slow) outflow of the pore water.

Let us focus on a point closest to the heat source wall at $r = 10{\cdot}6$ cm (1·1 cm away from the wall) at $M = \text{const}$ (Fig. 5). In response to the initial pore pressure growth, the effective mean stress decreases and an additional mechanical volumetric strain rate ensues, initially elastic and expansive, and then with a thermoplastic and compactive component. Such a scenario resembles a classical undrained triaxial thermal failure experiment, called Scenario II by Hueckel *et al.* (1987), Hueckel & Pellegrini (1991) and more recently by the authors (Hueckel *et al.*, 2009a). However, in the considered axisymmetric plane-strain boundary value problem, the displacements near the heater are constrained

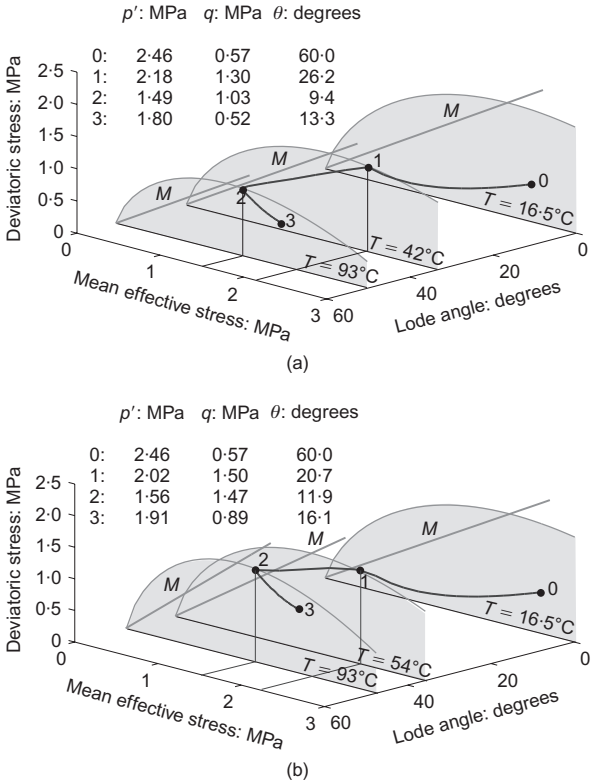

Fig. 5. Evolution of stress path in q, p', θ_L space in parallel with evolution of yield locus and critical state line for location $r = 10{\cdot}6$ cm (1·1 cm away from heat source wall): (a) for $M =$ constant; (b) for variable M

vertically and circumferentially, but are not constrained in the radial direction. Hence a marked principal stress difference (i.e. a deviatoric stress) develops in response to heating, not present in the above-mentioned experiment, conducted at $q = \text{const}$. The rising of this deviatoric stress critically affects the effective stress path, and is crucial in bringing the effective stress close to the critical state. This would not be the case for a plane-stress solution.

The above-described stress trajectory responds largely to the mentioned displacement constraints. The elastic segment 0–1 in Fig. 5, driven by the thermal pore pressure build-up, complies with the vertical strain boundary condition that $d\varepsilon_z^e = 0$. As in the undrained thermal failure case (Hueckel *et al.*, 2009a), this determines uniquely the elastic segment of the stress trajectory by way of the equality expressed in terms of the effective stress invariants as

$$\begin{aligned} d\varepsilon_z^e &= d\varepsilon_{11}^e \\ &= -\frac{1}{3}\beta_s dT + \frac{1}{3K} dp' + \frac{1}{3G}\cos\theta_L dq - \frac{q}{3G}\sin\theta_L d\theta_L \\ &= 0 \end{aligned} \tag{7}$$

The strains generated in the elastic regime are by definition independent of M, as seen above, except for the fact that the extent of the elastic regime itself is altered by the variation in M. As can be seen in Fig. 5, the effective stress path for variable M (Fig. 5(b)) reaches visibly higher values of q and slightly lower values of p' than those at a constant M (Fig. 5(a)). This is clearly a result of the influence of the variable M on the evolution of the yield locus, which develops a higher aspect ratio at high ΔT, in the former case. As an outcome, the response to the isotropic unloading

due to the pore water pressurisation is elastic over a longer part of the process than in the case of $M = \text{const}$. Consequently, yielding (point 1) starts at quite different temperatures: at $T = 42°C$ for $M = \text{const}$, and at 54°C for $M = M(\Delta T)$. In other words, the thermally induced increase of internal friction delays the onset of yielding by over 12°C in the considered boundary value problem.

Yielding opens the door to an interaction of three possible hardening mechanisms:

(*a*) apparent preconsolidation temperature softening, already active in the elastic range, postulated as monotonic, and characterised by the inequality $(\partial f/\partial p'_c)(\partial p'_c/\partial T) > 0$
(*b*) plastic strain-hardening
(*c*) a possible effect of the variation of the critical stress state (or friction angle variation), also already active in the elastic range.

The subsequent stress increment is a resultant of this interaction, and in this case is most likely to be directed inward of the yield locus of the moment. This produces an abrupt turnaround in the stress trajectory. When a compressive volumetric plastic strain rate arises, the plane-strain constraint changes into a rate condition, $d\varepsilon_z^p = -d\varepsilon_z^e$, which alters the course of the effective stress trajectory. Indeed, the above stated constraint, together with the consistency equation, determines the following stress increments. This can be best seen for the case of $M = \text{const}$.

$$df = \frac{\partial f}{\partial p'}dp' + \frac{\partial f}{\partial q}dq + d\Lambda \frac{\partial f}{\partial \varepsilon_v^p}\frac{\partial f}{\partial p'} + \frac{\partial f}{\partial p'_c}\frac{\partial p'_c}{\partial T}dT = 0 \tag{8}$$

$$d\Lambda\left[\frac{\partial f}{\partial p}\frac{1}{3} + \frac{\partial f}{\partial q}\sin(\theta_L)\right] = \frac{1}{3}\beta_s dT - \frac{1}{3K}dp' - \frac{1}{3G}\cos\theta_L dq + \frac{q}{3G}\sin\theta_L d\theta_L \tag{9}$$

Eliminating the multiplier $d\Lambda$, an incremental expression for the effective stress trajectory during the plasticity phase is arrived at expressed in terms of the invariants dq, dp' and $d\theta_L$ for a given temperature increment.

As the stress range in which the effective stress path reaches yielding (see Figs 5(a) and 5(b)) corresponds to the top parts of the yield loci, with a minuscule plastic volumetric strain component (i.e. the horizontal component of the local yield locus normal), the expected contribution from the plastic strain-hardening is indeed very small (compare Fig. 4).

As the stress point moves through plastic states near the critical locus, the volumetric component of the plastic strain rate progressively decreases even further. Notably, the case of variable M is characterised by the compensatory role carried mainly by $M(\Delta T)$ hardening: hence the overall softening is less evident. The $M = \text{const}$ case, in addition to a more evident softening, is characterised by reaching very close to the critical state line.

At 95°C the source temperature stops increasing (and hence so does the pore pressure) in the imposed heating programme, and soon after this the pore pressure starts to decrease, owing to water outflows. At the same time, the yield locus is arrested at the location corresponding to the maximum imposed temperature (point 2). Although the pore water stops expanding, it continues its outflow, but in a limited quantity, given that the pore pressure gradient is quite small. The pore pressure hence starts to decrease at a very low rate, while the effective stress state re-enters the elastic domain, producing an effective stress trajectory segment 2–3, nearly parallel to the original elastic loading segment 0–1.

It is interesting to note how short (in terms of time) the plastic episode is (e.g. seen as the segment of the variable volumetric plastic strain in Fig. 4), compared with the elastic unloading period driven by water pressure dissipation, but also how remarkable the plasticity effect is in terms of the change in the effective stress trajectory. Fig. 6 shows projections of the effective stress paths on the plane $\theta_L = 0°$, which is the plane of the initial stress state. As discussed earlier, the constitutive properties of the material are all independent of θ_L.

First, the conclusion from Fig. 5 can be now extended to further locations, indicating that thermoplastic yielding affects the effective stress path. The figures show also the differences between the effective stress trajectories at three locations within the plastic strain range, at a relatively small distance from the heat source (40 cm away from the interface at most). Most prominently, the figures demonstrate the difference in the evolution of the yield locus between the $M = \text{const}$ case and the variable-M case.

It is clear that when M grows, and hence the aspect ratio of the yield locus q_{max}/p_{max} increases, the value of the maximum deviatoric stress reached is higher, and the subsequent drop in the deviatoric stress component during the thermoplastic yielding process is consistently much more limited, than in the $M = \text{const}$ case. Hence the ensuing softening at a given location for a given stress history is much less pronounced, or practically non-existent, as seen in Fig. 7.

It is also instructive to note that only a portion of the pore pressure increase of about 1·2 MPa (1·24 MPa for constant M and 1·13 MPa for variable M) between the onset of yielding at point 1 and the end of yielding at point 2 is accommodated by the response in terms of the effective mean stress change, which is about 0·6 MPa (0·61 MPa for constant M and 0·59 MPa for variable M). The rest of the difference affects the total stress development. This can be seen in Fig. 6 as a difference in the abscissa between the respective points of the effective and total stresses, which corresponds exactly to the pore pressure value. Indeed, starting at the point of yielding (1), the total mean stress exhibits an abrupt increase for both cases of M, causing the total stress trajectory to make a turn. However, this turn is opposite to that exhibited by the effective stress path.

The corresponding deviatoric stress–strain curves are shown in Figs 7(a) and 7(b) for the two cases of M variability at the three locations. It is seen that in these cases there is a modest amount of the total deviatoric strain of about 0·5%, or 0·4% of which nearly $\frac{3}{4}$ is irreversible at the hottest location, 1·1 cm away from the wall, whereas there is scarcely any plasticity for the location at 40 cm from the heat source.

Interestingly, the variable M produces less deviatoric plastic strain, and clearly more elastic strain, as discussed above. The terminal amounts of deviatoric strain are nearly the same, but for the variable M case most of this is an elastic locked-in strain. While these amounts of permanent shear strain are not by any means large, they indicate that the material suffered a certain amount of damage in a zone of nearly 80 cm diameter around the heat source. Note that, in the problem studied, the weight of the heat source is not considered, for simplicity and the two-dimensional character of the problem. However, the weight of the heat source may become an issue, as it may increase the deviatoric stress and induce further deviatoric strain.

For more remote locations, at $r = 25·6$ and 50·4 cm, the effective and total stress paths shown in Fig. 6 present a somewhat different picture. For the variable-M case, the

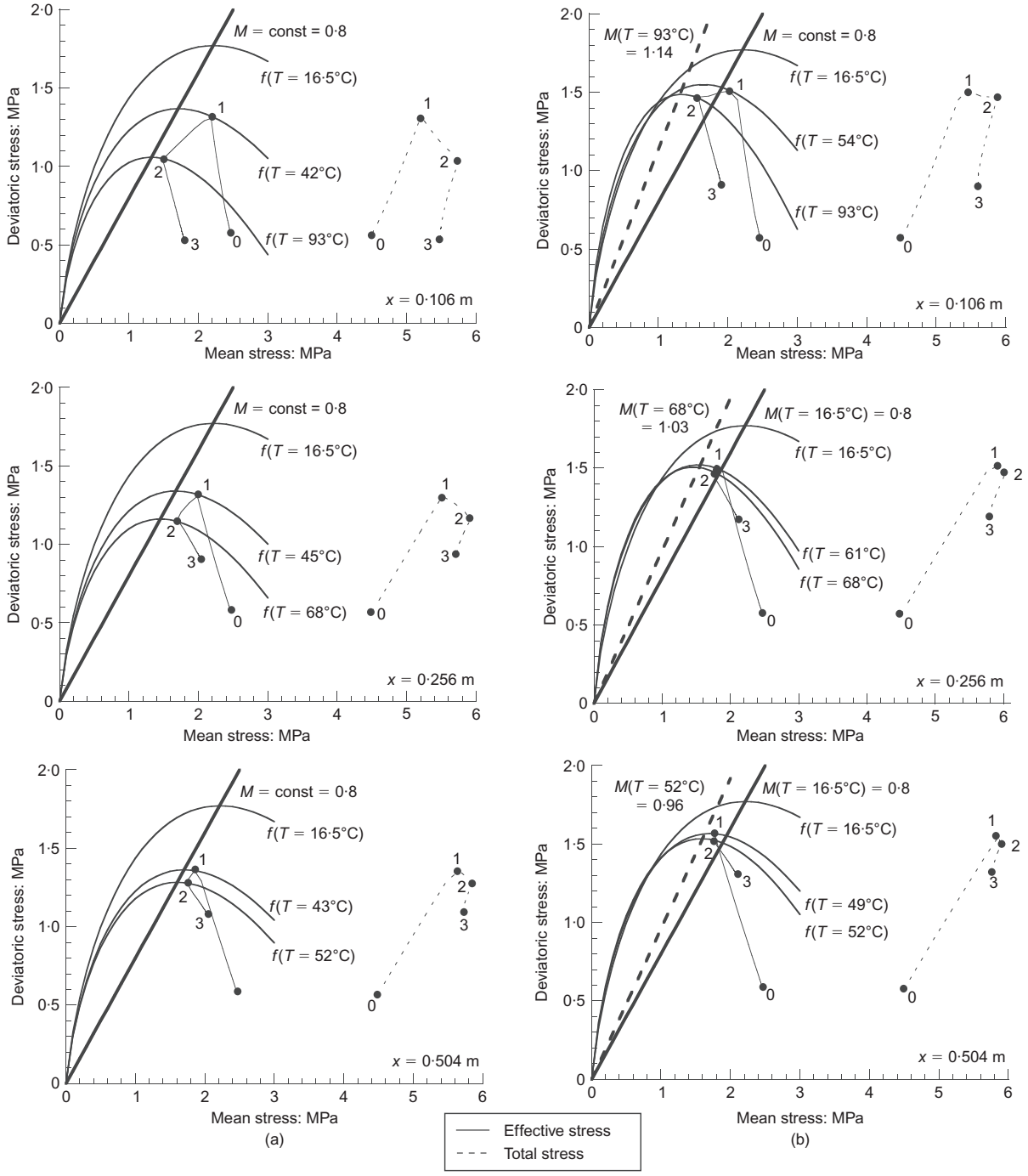

Fig. 6. Evolution of the stress path in q, p' space in parallel with evolution of yield locus and critical state line for different locations within zone of thermo-plasticity ($r = 10{\cdot}6$ cm, $r = 25{\cdot}6$ cm and $r = 50{\cdot}4$ cm): (a) for $M =$ constant; (b) for variable M

plasticity episode 1–2 is much less significant, with less plastic deviatoric strain. For the $M =$ const case there is more plasticity at both locations, and more deviatoric plastic strain.

Most remarkably, for both cases and for all three locations, the effective stress path comes very close to the critical state line, at the end of the plastic process and the maximum attained temperature. In terms of mean effective stress, the distance from the critical states amounts to as little as 0·1 MPa. While there is no established quantitative criterion for the margin of safety in such a situation, it certainly is not a healthy situation. In other words, the margin of safety, in whatever terms it is expressed, for these more remote locations is alarmingly low. Any adverse local material inhomogeneity or random load fluctuation may bring the effective stress trajectory to the other side of the critical state locus, where the material behaviour may become unstable, or non-unique, or statically inadmissible (Bigoni & Hueckel, 1991; Hueckel *et al.*, 2009b). Counter-intuitively, these locations are not locations where the highest (spatially) temperature or highest pore pressure is attained. The temperature value is much below the maximum at the heater of 96·5°C. Indeed, it is only 80°C at $r = 25{\cdot}6$ cm and 68°C at $r = 50{\cdot}4$ cm. Consequently, the total stress trajectory is much less articulated than its counterpart closer to the heater.

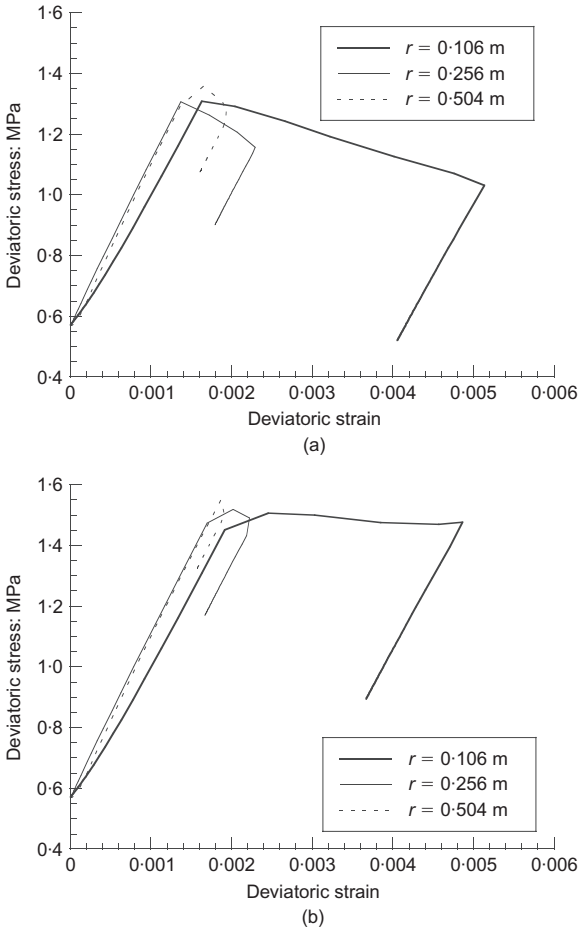

Fig. 7. Deviatoric stress–strain curve at locations near heat source, showing amount of plastic strain: (a) for $M =$ constant; (b) for variable M

Evolution of stress and strain state distribution

The deviatoric stress invariant distribution along the radius is shown in Fig. 8. During the elastic phase the distribution follows that of the temperature, with a maximum value near the contact with the heat source (at 10 days in Fig. 8). Soon after yielding starts, the value at the contact drops by almost half, and the maximum is at the interface between the elastic and plastic range.

The maximum growth in q is about 12·5% higher for the variable-M case. It is easy to see in the same figure that the yielding zone is more than twice as large in the $M =$ const case than for variable M: 1·8 m against 0·8 m.

As far as the individual effective stress components are concerned,. the evolution of axial stress (Fig. 9) is strongly related to the kinematic constraint of plane strain ($\varepsilon_z = 0$) and the generation of thermoelastic expansion first, and later accompanied by thermoplastic axial compression, which reduces the reacting compressive stress. Notably, upon entry into the plastic range, the plane-strain constraint, $\varepsilon_z = 0$, converts into a rate condition: $\mathrm{d}\varepsilon_z^{\mathrm{p}} = -\mathrm{d}\varepsilon_z^{\mathrm{e}}$. Both elastic and plastic axial strains have components proportional to temperature rate and the rate of change of the effective stress. The latter is influenced largely by the development of pore water pressure, owing to a substantial thermal expansion of water. Note that, as mentioned earlier, the pore pressure in the vicinity of the heat source ($r < 0{\cdot}5$ m) stops growing at 50 days, and after that starts to dissipate. This induces transfer of a portion of the load on to the solid phase (in terms of compressive effective stress). Interestingly, in contrast to the nearest vicinity of the heater, for radii larger than about 1·0 m the pore pressure increases monotonically all the time: see Fig. 2(b). As a result, the effective compressive stress also decreases there, albeit by less, because of the lower temperatures.

As a result, directly near the heat source wall, the axial effective stress initially increases in response to thermal expansion, and then after about 15 days drops by over 0·90 MPa with respect to the in situ value to 1·95 MPa, for the $M =$ const case. In the case of variable M, the drop is somewhat less (0·60 MPa) after about 20 days. Indeed, yielding occurs significantly later (as the yield locus changes its aspect ratio significantly). The drop is confined to about 0·5 m initially, and after about 50 days another development takes place in an outer ring of the plastic range, between radii of 0·8 and 0·2 m. The drop is clearly related to the appearance of plastic strains, which counteract the thermal expansion effect.

The onset of yielding, occurring after 30 days of heating,

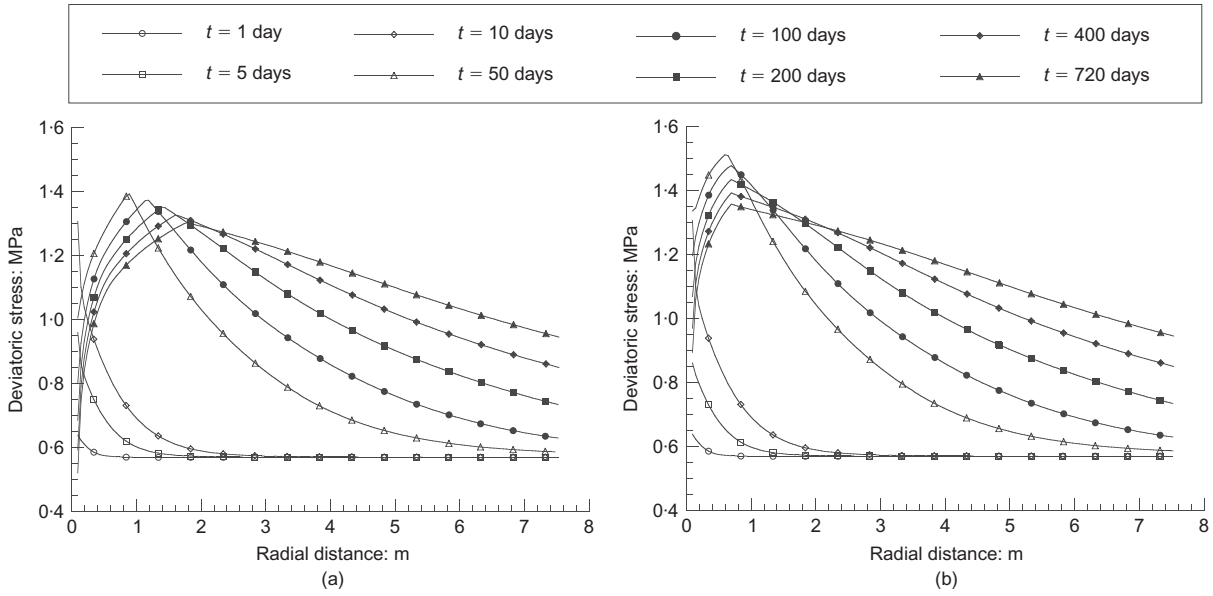

Fig. 8. Distribution of deviatoric stress invariant: (a) for $M =$ constant; (b) for variable M

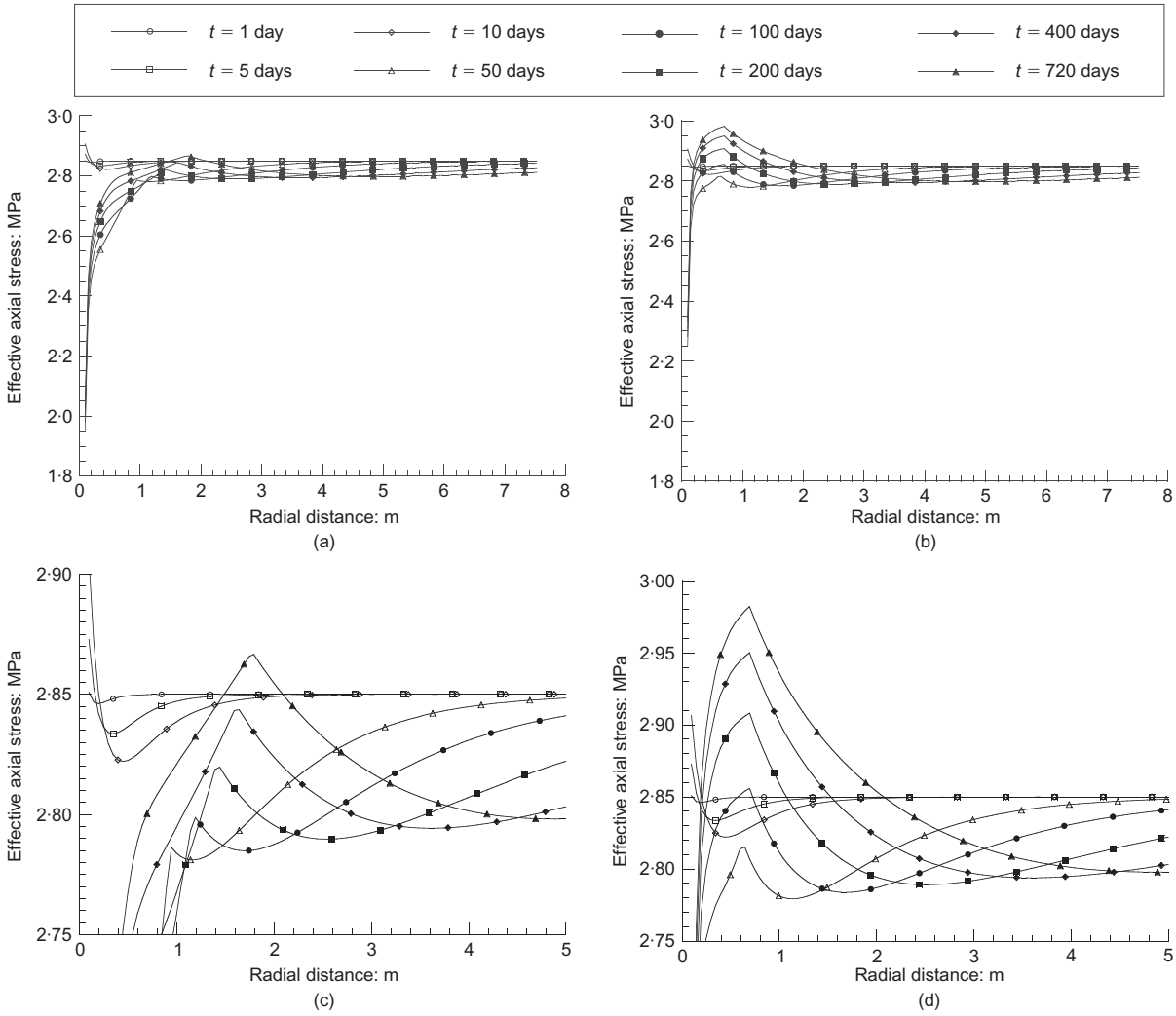

Fig. 9. Distribution of effective axial stress: (a) for $M =$ constant; (b) for variable M. (c) and (d) are magnifications of (a) and (b) respectively

leads to an abrupt and quite substantial change in axial effective stress distribution. Between day 10 and day 50 there is a 'rapid' change of about 0·8 MPa in axial stress.

For the case of variable M, the stress increases by over 0·2 MPa at the interface between the plastic and elastic zones, whereas in the $M =$ const case it generally drops, or increases imperceptibly, at the very end of the process. Consequently, the resulting range of axial stress affected by the thermoplastic developments is larger for the variable-M case (Fig. 9(b)), even if the plastic strain zone itself is smaller in the case of variable M, as seen in Figs 8(a) and 8(b) (the elasto-plastic interface position).

There are almost no differences between the two cases of M in terms of the horizontal radial effective stress distribution. Numerically, this effective stress component exhibits much higher changes than other components, that is, nearly 1·25 MPa, mainly concentrated in the plastic zone, and gradually fading out in more remote regions (Fig. 10(a)). The zone affected by a change of more than 0·50 MPa in effective horizontal radial stress is quite extensive in both cases: it reaches almost 8 m in diameter for variable M. More modest (and nearly identical to each other for the two cases of M) are the changes in horizontal circumferential effective stresses (Fig. 10(b)). A 0·5 MPa change extends over 16 m in diameter.

Implications for monitoring system design and spacing of heating devices

The conducted simulations make it possible to study the extent of the zones of influence of the triggered phenomena around a heat source. Proper assessment of such zones is crucial for rational design of monitoring systems. It is vital for meaningful monitoring to measure variables where they reach extreme values. A good monitoring system is also one that measures the variables using sensors with adequate sensitivity.

The numerical study presented here, although based on a set of actual data concerning the material properties of a specific clay, is not to be construed as a simulation of a specific technical project. Rather, it is to be treated as an academic study, not necessarily technically realistic. In particular, the contained analysis is only one-dimensional, the boundary conditions may not be realistic from the point of view of simulating the effect of a nuclear waste disposal facility on the clay mass (e.g. zero displacement at the contact with the heat source), and the heating programme may be too limited (lack of the cooling phase). This simulation also ignores the effects of the weight of the heat source. Depending on the type of heat-emitting device, and on the application in general, the weight effect may be crucial in a situation that involves thermoplastic yielding, damaging the closest neighbourhood

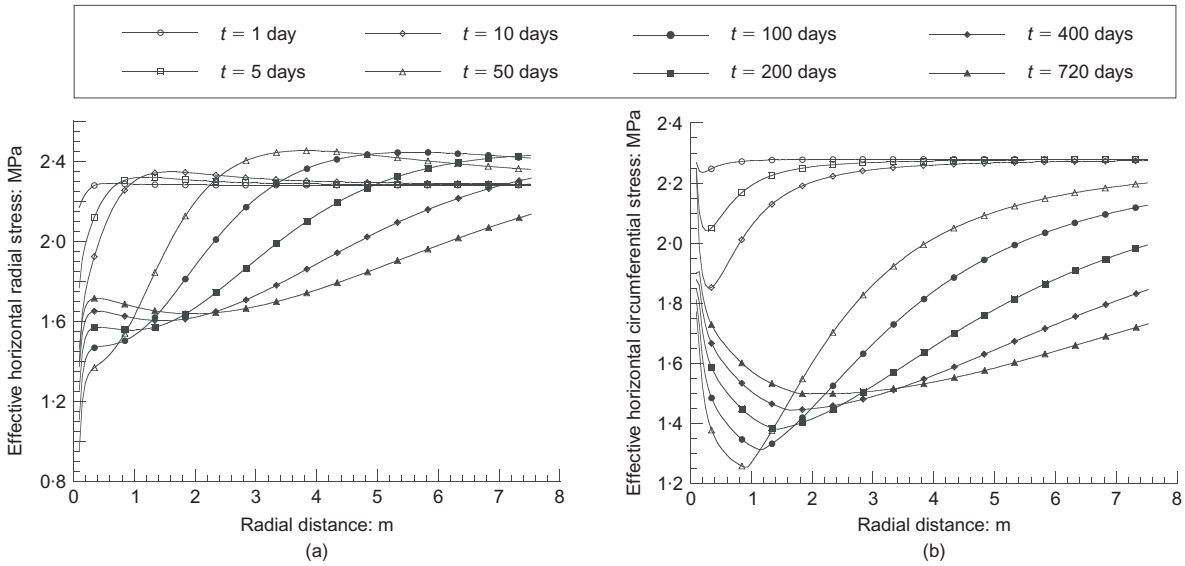

Fig. 10. Distribution of (a) horizontal radial and (b) horizontal circumferential effective stress components for variable M. Distributions for $M =$ constant differ minimally

of the heat source. Finally, the induced excavation damage zone (EDZ) due to the borehole production, which could have implications for the thermoplastic behaviour of the host material, has not been considered. Therefore the numerical values of the extent of the influence zones apply only to the boundary value problem being considered. However, the concept of the zone of influence, as depicted in Fig. 11 and discussed below, remains critical for good monitoring system design.

The size of the zone of influence of thermoplastic yielding (about 1·6 m in diameter) is most worrying from the point of view of the structural safety of the soil mass. Equally troublesome is the extent of the zone (about 1·0 m) in which the effective stress state is less than 0·1 MPa away in terms of the mean effective stress from the critical state. While a rigorous criterion for the safety margin is still to be established for a soil mass, this is probably the most critical finding from this simulation. The largest zone of influence (6·6 m in diameter) is that of the thermally elevated pore pressure of up to 1·5 MPa, and a significant change in the effective stress components.

The former finding is of particular relevance for the design of heat-generating facilities, where multiple heat sources may overlap in terms of their influence zones, giving rise to higher values in the areas of overlap, and affecting other parameters of the performance. It is customary to design such multi-source facilities based on a non-interaction criterion of the heat fields only. It is clear that the heat influence zone is the smallest of both the hydraulic and mechanical fields, hence rendering the heat non-interaction criterion the least safe criterion.

It is clear that any variable of interest should be monitored within its zone of influence, and with a sensor that is sufficiently sensitive to operate in the range indicated. Also, for the simulation of actual repositories, the ranges of the zones of influence will be affected by the actual heating programme (including cooling) corresponding to a variety of waste emplacement histories, and realistic boundary conditions, as well as a possible superposition of multiple heat sources.

Further considerations of thermal failure at the field scale

In the numerical simulations it was shown that, independently of the temperature dependence of coefficient M during heating up to 96·5°C, thermal pressurisation of the pore water brings the effective stress path very close to the critical state. Although the amount of associated irreversible deviatoric strain does not pose any threat to the embedded structure, small heterogeneities in material properties as well as small perturbations in the load parameters may easily cause a variation of the effective stress path, such that the stress state may migrate to the 'wet' side of the yield locus. This may lead to a possible instability, strain localisation and/or non-uniqueness of response, or alternatively a statically inadmissible response (Hueckel *et al.*, 2009b). First, such an occurrence is more likely to take place when $M =$ const, rather than when the material internal friction is thermally strengthened by temperature. Second, the likelihood of such an occurrence is at least equally plausible in the entire zone of plasticity. Indeed, in the considered case it is highest at the distance of 40·9 cm from the wall of the heat source, which is the most remote of the considered points in the yielding zone. Finally, in the studied case, the effective stress state is closest to the critical state at the end of the plastic process, which is arrested by an 'arbitrarily imposed' end of heating. The notion of a thermal global failure is still awaiting a rigorous treatment, but what probably is true is that the aforementioned local criterion is a necessary condition for a global failure to take place. No rigorous criteria exist for thermomechanical instability, especially in the presence of pore pressure. An attempt was made by Benallal & Bigoni (2004), but limited to isothermal and adiabatic processes, which would not apply to the present boundary value problem. In this paper the authors have adopted an intuitive criterion of a 'mean effective stress distance from the critical state' as a measure of instability. The issues of proper local (and global) criteria of thermoplastic stability, as well as that of margin of safety in a boundary value problem, critically require further intense attention.

As for the influence of the temperature dependence of the internal friction (and the coefficient of the critical state M) with temperature, the main findings are as follows. The biggest impact of the evolution of the internal friction is on the effective stress trajectory. In general, as might be expected, the growth of the internal friction lowers the possibility that the effective stress may reach the critical state. This happens mainly because a higher internal friction allows a larger portion of the response to be elastic, by

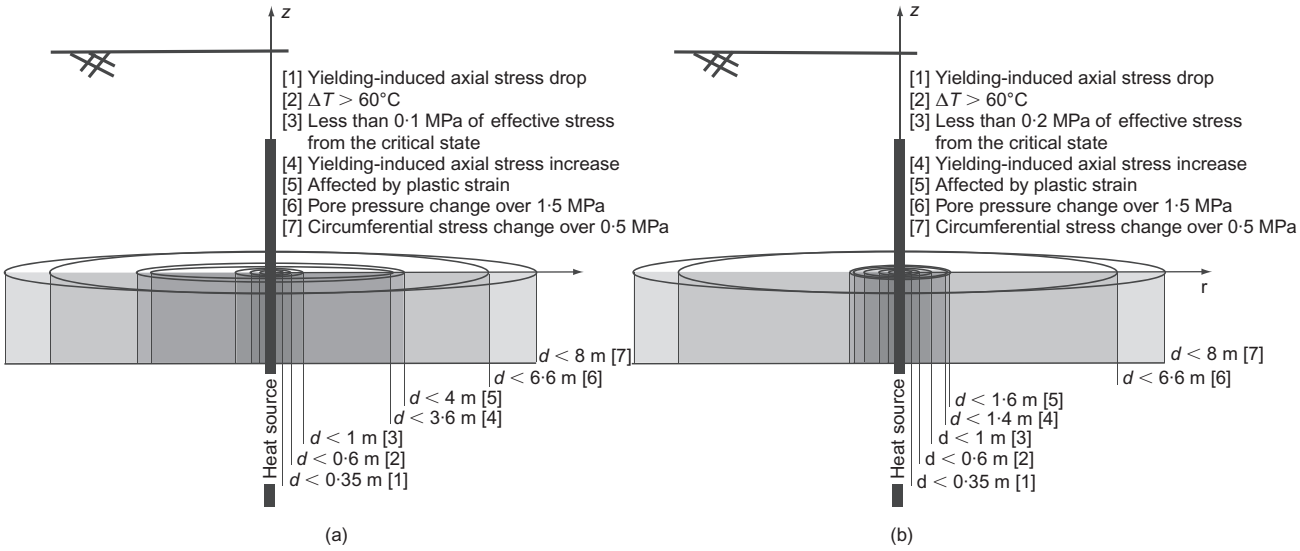

Fig. 11. The extent of zones of interest in considered case study: (a) for M = constant; (b) for variable M

increasing the aspect ratio of the yield locus. Second, the increasing friction angle decreases almost by half the zone of influence of axial stress alteration around the heat source. Finally, the rising internal friction reduces, again almost by half, the amount of deviatoric plastic strain at the most heated locations. As is seen, even if the thermal increase in the internal friction is quite modest (less than 20% in terms of M), its effect on several key quantificators of the solution of prime importance to the mechanical behaviour of the soil mass around the heat source may be paramount, such as reducing by half the extension of the plastic zone. This emphasises the need for attention to be paid to proper detection and quantification of a possible thermally induced variation of this soil characteristics.

CONCLUSIONS

The performed simulations, which use the actual parameters identified for a numerical model of an actual clay, make it possible to reveal

(*a*) general features of the mechanical fields generated by a heat source in the clay mass surrounding it, and in particular the proximity of the stress state to failure condition
(*b*) the effect of the dependence of one of the key soil mechanical parameters, the internal friction, on temperature
(*c*) a quantitative extent of the influence zones of various variables of relevance.

The first of the above findings is of paramount importance in such applications as geological nuclear waste disposal and underground heat storage, and emphasises the need for more attention to be paid to the margin of safety of the heat source embedded in the soil. The second finding suggests that even a relatively modest thermal sensitivity of a key parameter may play a large role in a boundary value problem (that is, at the field scale). Previous laboratory studies have shown that this temperature dependence is not very strong. Indeed, in many experimental studies on different soils it was considered to be marginally significant. However, several known clay materials consistently exhibit a response that, without considering a thermal dependence of internal friction, would at least be confusing.

The last finding offers a foundation for rational design of the relevant monitoring system in a heated soil mass. It is also crucial for the design of spacing of heat emitters ensuring limited superposition of a series of effects of neighbouring devices. It is clear that designing the heat source spacing based on the temperature field alone is quite inadequate. We have furthermore shown that the thermoplastic effects produce an increase of the thermally induced excess pore water pressure with a subsequent increase of water flux. This has very important implications for potential mass transport of a possible prematurely released radioactive contaminant in a nuclear waste repository. Hence proper identification of the amplitude of thermoplastic processes is of critical importance.

It is sometimes argued in the nuclear waste disposal community that a thermal pressurisation pulse of pore water around the heat source is irrelevant, because of its short duration. There is merit in this statement from the hydraulics (or a potential radionuclide transport) point of view. However, analysis of the resulting effective stress trajectory shows that, despite its short duration, the pore pressure increase causes the effective stress path to approach the critical state, and hence substantially reduces the structure's margin of safety. While the present study is not a simulation of a nuclear waste disposal facility, the relevance of the effective stress path should not be missed in stress analyses of repositories. Indeed, the simulations suggest that for some actual materials at a realistic initial state and some boundary conditions it is quite possible that the effective stress near the heat source may be quite close to the critical state.

ACKNOWLEDGEMENTS

Frederic Collin of the University of Liege (Belgium) is acknowledged for his contribution in the discussions of the results of the simulations. Tomasz Hueckel acknowledges the invitation and support of EPFL during his Visiting Professorship in June and July 2009 while working on this paper at the Laboratory of Soil Mechanics.

NOTATION

$c_{p,w}$ heat capacity of water
$c_{p,s}$ heat capacity of solid
e void ratio
e_0 initial void ratio
f yield limit
G incremental shear modulus

g parameter for evolution of slope of critical state line with temperature
K incremental bulk modulus
K_0 coefficient of earth pressure at rest
k_w water permeability
M slope of critical state line in $p'-q$ plane
m' exponent for evolution of incremental shear modulus with mean effective stress
n porosity
n' exponent for evolution of incremental bulk modulus with mean effective stress
p' mean effective stress
p'_c preconsolidation pressure
p'_{c0} initial apparent preconsolidation pressure
p_{max} major semi-axis of yield locus
p_w pore water pressure
q deviatoric stress
q_{max} minor semi-axis of yield locus
T temperature
T_0 initial temperature
ΔT temperature variation
u displacement
α^T material parameter for evolution of dynamic viscosity of water with temperature
β plastic compressibility of soil
β'_s volumetric thermal expansion coefficient of solid
β'_w volumetric thermal expansion coefficient of water
γ material parameters for evolution of preconsolidation pressure with temperature
$\tilde{\varepsilon}^e$ elastic strain
$\tilde{\varepsilon}^p$ plastic strain
θ_L Lode angle
Λ plastic multiplier
λ_s thermal conductivity of solid
λ_w thermal conductivity of water
μ_{w0} dynamic viscosity of water at initial temperature
ρ_s bulk density of solid
ρ_{w0} initial bulk density of water
$\tilde{\sigma}$ total stress
$\tilde{\sigma}'$ effective stress
ϕ' internal friction angle
χ_w bulk modulus of water

Subscripts

d deviatoric
r radial (horizontal)
t circumferential (horizontal)
v volumetric
z axial (vertical)

REFERENCES

Baldi, G., Hueckel, T. & Pellegrini, R. (1988). Thermal volume change of the mineral-water system in low-porosity clay soils. *Can. Geotech. J.* **25**, No. 4, 807–825.

Baldi, G., Hueckel, T., Peano, A. & Pellegrini, R. (1991). *Developments in modelling of thermo-hydro-mechanical behaviour of Boom clay and clay-based buffer materials*, Vols 1 and 2, EUR 13365/1 and 13365/2. Luxembourg: Commission of the European Communities.

Bastiaens, W., Bernier, F. & Li, X. L. (2006). An overview of long-term HM measurements around HADES URF. *Proceedings of EUROCK 2006: Multiphysics Coupling and Long Term Behaviour In Rock Mechanics, Liège*, 15–26.

Benallal, A. & Bigoni, D. (2004). Effects of temperature and thermo-mechanical couplings on material instabilities and strain localization of inelastic materials. *J. Mech. Phys. Solids* **52**, No. 3, 725–753.

Bernier, F., Li, X. L. & Bastiaens, W. (2007). Twenty-five years' geotechnical observation and testing in the Tertiary Boom Clay formation. *Géotechnique* **57**, No. 2, 229–237, **doi**: 10.1680/geot.2007.57.2.229.

Bigoni, D. & Hueckel, T. (1991). Uniqueness and localization: I. Associative and non-associative elastoplasticity. *Int. J. Solids Structs* **28**, No. 2, 197–213.

Booker, J. R. & Savvidou, C. (1985). Consolidation around a point heat source. *Int. J. Numer. Analyt. Methods Geomech.* **9**, No. 2, 173–184.

Borsetto, M., Peano, A., Pellegrini, R., Mazza, G. & Pedroni, G. (1993). Numerical simulation of thermo-hydro-elasto-plastic behaviour of clay mass in a nuclear waste repository. *Proceedings of the international workshop on thermo-mechanics of clays and clay barriers*, Seriate (Bergamo), Session 3, pp. 1–23.

Britto, A. M., Savvidou, C., Maddocks, D. V., Gunn, M. J. & Booker, J. R. (1989). Numerical and centrifuge modeling of coupled heat-flow and consolidation around hot cylinders buried in clay. *Géotechnique* **39**, No. 1, 13–25, **doi**: 10.1680/geot.1989.39.1.13.

Carter, J. P. & Booker, J. R. (1989). Finite element analysis of coupled thermoelasticity. *Comput. Structs* **31**, No. 1, 73–80.

Cekerevac, C. & Laloui, L. (2004). Experimental study of thermal effects on the mechanical behaviour of a clay. *Int. J. Numer. Analyt. Methods Geomech.* **28**, No. 3, 209–228.

Charlier, R. (1987). *Approche unifiée de quelques problèmes non linéaires de mécanique des milieux continus par la méthode des éléments finis*. PhD thesis, Université de Liège, Belgium.

Charlier, R., Radu, J. P. & Collin, F. (2001). Numerical modelling of coupled transient phenomena. *Rev. Fr. Génie Civ.* **5**, No. 6, 719–741.

Chen, W. F. & Han, D. A. (1988). *Plasticity for structural engineering*. New York, NY, USA: Springer-Verlag.

Collin, F. (2003). *Couplages thermo-hydro-mécaniques dans les sols et les roches tendres partiellement saturés*. PhD thesis, Université de Liège, Belgium.

Collin, F., Li, X., Radu, J. P. & Charlier, R. (2002). Thermo-hydro-mechanical coupling in clay barriers. *Engng Geol.* **64**, Nos 2–3, 179–193.

François, B., Laloui, L. & Laurent, C. (2009). Thermo-hydro-mechanical simulation of ATLAS in-situ large scale test in Boom Clay. *Comput. Geotech.* **36**, No. 4, 626–640.

Gawin, D., Baggio, P. & Schrefler, B. A. (1995). Coupled heat, water and gas-flow in deformable porous-media. *Int. J. Numer. Analyt. Methods Fluids* **20**, Nos 8–9, 969–987.

Giraud, A. (1993). *Thermo-hydro-mechanical couplings in low permeability porous media: application to deep clays*. PhD thesis, ENPC, Paris.

Goodier, J. N. (1937). On the integration of the thermo-elastic equations. *Phil. Mag.* **23**, No. 157, Special Issue 7th Series, 1017–1032.

Hueckel, T. & Baldi, G. (1990). Thermoplasticity of saturated clays: experimental constitutive study. *J. Geotech. Engng* **116**, No. 2, 1778–1796.

Hueckel, T. & Borsetto, M. (1990). Thermo-plasticity of saturated soils and shales: constitutive equations. *J. Geotech. Engng* **116**, No. 12, 1778–1796.

Hueckel, T. & Pellegrini, R. (1991). Thermoplastic modeling of undrained failure of saturated clay due to heating. *Soils Found.* **31**, No. 3, 1–16.

Hueckel, T. & Pellegrini, R. (1992). Effective stress and water pressure in saturated clays during heating-cooling cycles. *Can. Geotech. J.* **29**, No. 6, 1095–1102.

Hueckel, T., Borsetto, M. & Peano, A. (1987). Modelling of coupled thermo-elasto-plastic-hydraulic response of clays subjected to nuclear waste heat. In *Numerical methods in transient and coupled problems* (eds R. W. Lewis, E. Hinton, P. Bettess and B. A. Schreffler), pp. 213–235. Chichester: John Wiley.

Hueckel, T., François, B. & Laloui, L. (2009a). Explaining thermal failure in saturated clays. *Géotechnique* **59**, No. 3, 197–212, **doi**: 10.1680/geot.2009.59.3.197.

Hueckel, T., Laloui, L. & François, B. (2009b). Implications of thermal sensitivity of the static internal friction angle. *Proc. 1st Int. Symp. on Computational Geomechanics (ComGeo I), Juan-les-Pins*, 104–115.

Hujeux, J. C. (1985). Une loi de comportement pour le chargement cyclique des sols. In *Génie parasismique* (eds V. Davidovici *et al.*), pp. 287–303. Paris: Les éditions de l'E.N.P.C.

Laloui, L. (1993). *Modélisation du comportement thermo-hydro-mécanique des milieux poreux anélastique*. PhD thesis, Ecole Centrale de Paris.

Laloui, L. & Cekerevac, C. (2003). Thermo-plasticity of clays: an isotropic yield mechanism. *Comput. Geotech*. **30**, No. 8, 649–660.

Laloui, L. & François, B. (2009). ACMEG-T: soil thermo-plasticity model. *J. Engng Mech*. **135**, No. 9, 932–944.

Lewis, R. W. & Schrefler, B. A. (1987). *The finite element method in the deformation and consolidation of porous media*. Chichester: John Wiley & Sons.

Ma, C. M. & Hueckel, T. (1993). Thermomechanical effects on adsorbed water in clays around a heat-source. *Int. J. Numer. Analyt. Methods Geomech*. **17**, No. 3, 175–196.

McTigue, D. F. (1986). Thermoelastic response of fluid-saturated porous rock. *J. Geophys. Res*. **91**, No. B9, 9533–9542.

Olivella, S., Carrera, J., Gens, A. & Alonso, E. E. (1994). Non-isothermal multiphase flow of brine and gas through saline media. *Transp. Porous Media* **15**, No. 3, 271–293.

Picard, J. M. (1994). *Ecrouissage thermique des argiles saturées: application au stockage de déchets radioactifs*. PhD thesis, ENPC, Paris.

Prager, W. (1958). Non-isothermal plastic deformation. *K. Ned. Akad. Wet. Te Amsterdam B* **61**, 176–182.

Schofield, A. & Wroth, P. (1968). *Critical state soil mechanics*. London: McGraw-Hill.

SCK-CEN (1997). *HADES tour guide*. Notebook, 5th edn.

Seneviratne, H. N., Carter, J. P. & Booker, J. R. (1994). Analysis of fully coupled thermomechanical behaviour around a rigid cylindrical heat source buried in clay. *Int. J. Numer. Analyt. Methods Geomech*. **18**, No. 3, 177–203.

Timoshenko, S. P. & Goodier, J. N. (1934). *Theory of elasticity*. New York: McGraw-Hill.

Zhou, Y., Rajapaske, K. N. D. & Graham, J. (1998). Coupled consolidation of a porous medium with a cylindrical or a spherical cavity. *Int. J. Numer. Analyt. Methods Geomech*. **22**, No. 6, 449–475.